



Intracerebroventricular streptozotocin induces impaired Barnes maze spatial memory and reduces astrocyte branching in the CA1 and CA3 hippocampal regions

María F. Zappa Villar¹ · Juliette López Hanotte¹ · Eugenia Falomir Lockhart¹ · Lucía S. Trípodí¹ · Gustavo R. Morel¹ · Paula C. Reggiani¹ 

Received: 13 May 2018 / Accepted: 12 September 2018 / Published online: 22 September 2018
© Springer-Verlag GmbH Austria, part of Springer Nature 2018

Abstract

Sporadic Alzheimer's disease (SAD) is the most common form of dementia; therefore, there is an urgent need for a model that recapitulates the main pathologic hallmarks of this disease. The intracerebroventricular (icv) injection of streptozotocin (icv-STZ) in rats constitutes a promising model, and thus, icv-STZ rats develop insulin-resistant brain state and cognitive impairments. Even though a great piece of studies has hitherto described this system as a model for SAD, further behavioral and morphometric studies are still needed to fully characterize it. In this study, using *Sprague Dawley* rats, we evaluated short-term effects on behavior and hippocampus morphometry of the icv-STZ injection at two doses: 1 (STZ1) and 3 mg/kg (STZ3). We found that, following icv-STZ injection, STZ3 animals, but not STZ1, exhibited impairments in spatial reference learning and memory (Barnes maze test) and in recognition memory (object recognition test). Furthermore, the results from behavioral and morpho-histochemical data are compatible. STZ3 rats displayed *Stratum Radiatum* volume reduction and a decreased NeuN immunoreactivity (neuron loss) in hippocampal CA1 region, together with an increased immunoreactivity for microglial (Iba1) and astroglial (GFAP) markers (neuroinflammation). Sholl analysis revealed the vulnerability of hippocampal astrocytes to STZ in CA1 and CA3. Thus, both doses induced a reduction in process length and in the number of main processes, accompanied by a frank decrease in branching complexity. The present study provides important knowledge of this AD rat model. Overall, we found that the only high STZ dose induced severe and acute neurodegenerative lesions, associated with an inflammation process.

Keywords Sporadic Alzheimer's disease · Non-transgenic rat model · Streptozotocin · Spatial memory · Hippocampal morphology · Astrocyte-branching complexity

Introduction

Sporadic Alzheimer's disease (SAD) is the most frequent neurodegenerative pathology (Querfurth and LaFerla 2010), with high prevalence and morbidity, and at present, there are no effective therapies to reverse its progression. This

situation has caused an increasing problem of significant social, medical, and financial impact.

SAD is accompanied by progressive memory deficit, cognitive impairment, and personality changes. It is characterized by the formation of amyloid plaques and intraneuronal neurofibrillary tangles, neuronal degeneration, and alteration of cerebral energy metabolism (Schubert et al. 2004). The combination of an early diagnosis and an effective therapy is essential to curb the ongoing increase in the prevalence of the disease caused by higher life expectancy.

As a contribution to overcome this problem, numerous in vitro and in vivo animal models are being studied. A proposed rodent model of SAD is the intracerebroventricular (icv) administration of a diabetogenic drug, streptozotocin (STZ) (Lannert and Hoyer 1998; de la Monte et al. 2006; Salkovic-Petrisic and Hoyer 2007; Salkovic-Petrisic et al.

✉ Paula C. Reggiani
paulareggiani@conicet.gov.ar

María F. Zappa Villar
florz87@hotmail.com

¹ Institute for Biochemical Research (INIBIOLP)-Cathedral of Histology B, School of Medical Sciences, National University of La Plata (UNLP), CC 455, Zip 1900 La Plata, Argentina

2009). This non-transgenic model recapitulates the hallmark lesions of SAD (Selkoe 2001); indeed, the icv administration of STZ (icv-STZ) leads to an insulin-resistant state, selectively in the brain but not in the periphery (Salkovic-Petrisic and Hoyer 2007; Salkovic-Petrisic et al. 2009; Mayer et al. (1990), together with changes in brain glucose metabolism (Duelli et al. 1994; Heo et al. 2011), oxidative stress (Nunomura et al. 2006), increased amyloidogenesis (Salkovic-Petrisic et al. 2011), tau hyperphosphorylation (Grünblatt et al. 2007), cholinergic neuronal degeneration (Blokland and Jolles 1993; Hellweg et al. 1992), and memory impairments (de la Monte et al. 2006; Rostami et al. 2017; Shoham et al. 2003, 2007).

Different types of maze tasks are used to detect cognitive deficits in the icv-STZ rat model of SAD (Knezovic et al. 2015; Deshmukh et al. 2016; Isik et al. 2009). Spatial learning and reference memory were frequently studied in the Morris water maze (MWM) test (Deshmukh et al. 2016; Isik et al. 2009; Song et al. 2014; Gao et al. 2014). In 1979, Carol Barnes developed this dry-land maze to analyze a hippocampus-dependent cognitive task in senescent rats (Barnes 1979). Our group previously validated a variant of the BM protocol (Morel et al. 2015) to study cognitive aging. Here, this test is used to compare the effects of the two distinct doses of icv-STZ (1 and 3 mg/kg) in rats to evaluate spatial learning and reference memory. In addition, to expand our cognitive evaluation, we assess recognition memory in an also hippocampus-dependent benchmark task, the novel object recognition (NOR) test (Hashemi-Firouzi et al. 2017).

There is evidence of the degenerative effects of Alzheimer's disease (AD) among the different hippocampal subfields and their correlation with global cognitive function and memory performance (Su et al. 2018). One of these vulnerable regions in AD patients is the *Stratum Radiatum* (SR) (West et al. 1994), which is intimately involved in the pathways between *Cornu Ammonis* 1 (CA1) and CA3/entorhinal cortex, and between hippocampus and wider cortical areas. Consequently, SR and *pyramidal layer* of CA1 are considered candidate regions as AD biomarker (Su et al. 2018; West et al. 1994; Irvine et al. 2008). However, other hippocampal regions can show the signs of damage in AD. Among these regions are the dentate gyrus (DG), where the granular cells and astrocytes present morphological changes (Llorens-Martín et al. 2014) and CA3, which has shown neuronal density loss (Padurariu et al. 2012).

In addition, there is a critical need to study the association between specific functional glial states and AD progression, and, on the other hand, there is evidence that variation in glial extracellular environment causes glial morphology modifications that are closely linked to their function (Kreutzberg 1996; Montgomery 1994). Notwithstanding, astroglial changes during SAD progression are poorly

explored due to the lack of a suitable animal model for this disease was absent for many years. The mentioned icv-STZ rat model could contribute to overcome these needs. However, no studies have been yet to determine whether astrocyte morphology is altered by exposure to icv-STZ.

In the present study, we analyzed SR volume and morphological changes of neurons, ionized calcium-binding adaptor molecule 1 (Iba1)-positive microglia, and glial fibrillary acidic protein (GFAP)-positive astrocytes in the dorsal hippocampus after the exposure to low and high STZ doses.

Materials and methods

Animals

Three-month-old male *Sprague–Dawley* (SD) rats weighing 280–330 g (INIBIOLP, School of Medicine, University of La Plata, La Plata city, Argentina) were used throughout the studies.

Animals were housed 3 per cage in a temperature-controlled room (22–24 °C) on a 12 h light/12 h dark cycle (lights on 7 am–7 pm) with food and water available ad libitum.

Experiments were performed following the Animal Welfare Guidelines of NIH (INIBIOLP's Animal Welfare Assurance No A5647-01). The ethical acceptability of the animal protocols used here has been approved by our institutional IACUC (Protocol # T10-01-2013).

Surgical procedures

Rats were anesthetized with ketamine hydrochloride (40 mg/kg; ip) plus xylazine (8 mg/kg; im) and placed in a stereotaxic apparatus. Stainless-steel guide cannulas (a 21-gage needle) were placed directed toward the lateral ventricles. The stereotaxic coordinates for icv infusion were measured as 0.92 mm posterior to bregma; 1.5 mm lateral to sagittal suture; 3.9 mm beneath the brain surface (Paxinos and Watson 1998). Guide cannulas were fixed with dental cement. Following surgery, a single dose of ampicillin was injected. After the experiment, the location of the guide cannulas into the lateral ventricles was confirmed.

Spatial memory assessment

The modified Barnes maze (BM) protocol used here was previously documented (Morel et al. 2015). It involves three phases: habituation, training (acquisition trials), and probe, and consists of an elevated (108 cm to the floor) black acrylic circular platform, 122 cm in diameter, containing 20 holes around the periphery. The holes are of uniform

diameter (10 cm) and appearance, but only one hole is connected to a black escape box. The escape box is 38.7 cm long \times 12.1 cm wide \times 14.2 cm in depth and is removable. A white cylindrical starting chamber (an opaque, 25 cm in diameter and 20 cm high, open-ended chamber) is used to place the rats on the platform with a random orientation of their bodies. Four proximal visual cues are placed in the room, 50 cm away from the circular platform. The escape hole is numbered as Hole 0 for graphical normalized representation purposes, while the remaining holes are numbered 1–10 clockwise, and –1 to –9 counterclockwise (Fig. 2h).

During the whole experiment, hole 0 remained in a fixed position to avoid randomization of the relative position of the escape box. A 90-dB white-noise generator and a white-light 500-W bulb provided the escape stimuli from the platform. At the beginning of the experiment, rats were habituated to the task. The habituation routine consists of placing the animals in every compartment during 180 s (starting chamber and escape box). An acquisition trial (AT) consists of placing a rat in the starting chamber, located at the center of the platform for 30 s; the chamber is then raised, the aversive stimuli (bright light and high pitch noise) are switched on, and the rat is allowed to freely explore the maze for 120 s. The purpose of ATs is to train the rats to find the escape hole. A probe trial (PT) is similar to an AT except that the escape box is now removed; its purpose is to assess recent spatial memory retention. During PTs, rats explore the maze for 120 s. Behavioral performance was recorded using a computer-linked video camera mounted 110 cm above the platform. Subject performance was determined using the Kinovea v0.7.6 (<http://www.kinovea.org>) software. Behavioral parameters assessed were as follows:

- (a) *Latency*: Time (in s) spent by an animal since its release from the start chamber until it enters the escape box (during an AT), or until the first exploration of the escape hole (during a PT).
- (b) *Errors*: Number of explorations of holes different from the escape one until it enters the escape box (during an AT), or until the first exploration of the escape hole (during a PT). Each exploration of an incorrect hole is counted as an error, provided that the rat lowers its nose below the plane of the table surface.
- (c) *Total exploration frequency*: the sum of explorations number for each hole of the maze, during a PT.
- (d) *Exploration frequency in Goal Sector (GS)*: the sum of explorations number for holes –1, 0, and 1 divided by 3, during a PT.
- (e) *Search Paths* (Pompl et al. 1999): the search paths were classified as *spatial*, *serial*, and *random* as described by Barnes (1979). Briefly, spatial is moving directly toward the escape hole from the center of the maze without visiting holes more than two holes away from

the escape hole; serial is moving around the edge of the maze past at least three adjacent holes and random is searching in a nonsystematic search with multiple crossings through the center of the maze. The overall strategy score for one rat was generated as follows: spatial = 1, serial = 2, and random = 3, and this score was evaluated every 2 acquisition days. The search strategy was analyzed using the percentage of trials in which each strategy was used and was evaluated every two acquisition days (2 days/evaluation).

Recognition memory assessment

The novel object recognition (NOR) test is based on the ability of rats to show preference for novel versus familiar objects. On day 1, rats were individually habituated (120 s) to an open arena (square box, 65 \times 65 \times 45 cm). On day 2, the training session (120 s), two identical objects (termed as objects FO1 and FO2) were placed into the arena. On day 3, the recognition session (120 s), rats were placed back into the same arena, in which one of the objects was replaced by a novel object (NO) of similar dimensions but a different shape/color. Exploration behavior was assessed by quantifying the time spent exploring each object (Nanfaro et al. 2010).

Exploration was defined as the orientation of animal's snout toward the object, within a range of 2 cm or less from the object. The objects and the floor were carefully cleaned with ethanol (10%) after each individual trial to equate olfactory cues. Behavioral performance was recorded using a computer-linked video camera. Subject performance was determined using the Kinovea v0.7.6 (<http://www.kinovea.org>) software. NOR test measurements were as follows: (a) total time spent exploring two identical objects in the training session, and (b) total time spent exploring the novel object in the recognition session. Discrimination between the familiar and the novel object during recognition session was measured by comparing time spent exploring the familiar object versus time spent exploring the novel object.

Experimental design

A guide cannula was icv implanted in all animals 1 week before the STZ injection. Then, on the experimental day 0 (ED 0), 18 animals were randomly divided into three groups, six animals each: I-Sham, each rat received bilaterally 5 μ l of artificial cerebrospinal fluid (aCSF) containing 120 mM NaCl, 3 mM KCl, 1.15 mM CaCl₂, 0.8 mM MgCl₂, 27 mM NaHCO₃, and 0.33 mM NaH₂PO₄, adjusted to pH 7.4; II-STZ1, each rat received a bilateral icv injection of STZ (Sigma-Aldrich, CAS 18883-66-4) 1 mg/kg; III-STZ3, each rat received a bilateral icv injection of STZ 3 mg/kg. Drug concentration was adjusted

according to the animal body weight, and a volume of 5 μl /ventricle was administered using a 10 μl Hamilton syringe inside the cannulas. Changes in body weight were monitored and evaluated at 48 h interval. On the ED 13, rats were submitted to the Barnes maze protocol for 4 days, the habituation plus 3 days involving two ATs. Twenty-four hours after the last AT (AT6), on ED 17, rats were submitted to a PT (PT1). To follow further cognitive performance, 4 days after PT1, rats were submitted to a second PT (PT2). For the NOR test protocol, rats were individually habituated to the open arena on ED 22. On the following day, the training session was performed. After 24 h, rats were submitted to the recognition session. On the last experimental day (ED 25), all rats were euthanized by rapid decapitation (Fig. 1a).

Brain processing

Brains were quickly removed and divided into right and left hemispheres. The left hemispheres were fixed in phosphate-buffered para-formaldehyde 4%, (pH 7.4) overnight at 4 $^{\circ}\text{C}$. Afterwards, brains were kept in cryoprotectant solution (30% ethylene glycol, 1% polyvinylpyrrolidone, 30% sucrose, in phosphate buffer 0.1 M, and pH 7.4) at -20°C until use for immunohistochemistry. In the right brain hemispheres, the hippocampus was carefully dissected as previously described (Glowinski and Iversen 1966) and stored at -80°C until Western blot (WB) analysis.

Immunohistochemistry

Left brain hemispheres were cut coronally in 40 μm -thick sections with a vibratome (VT1000S; Leica Microsystems).

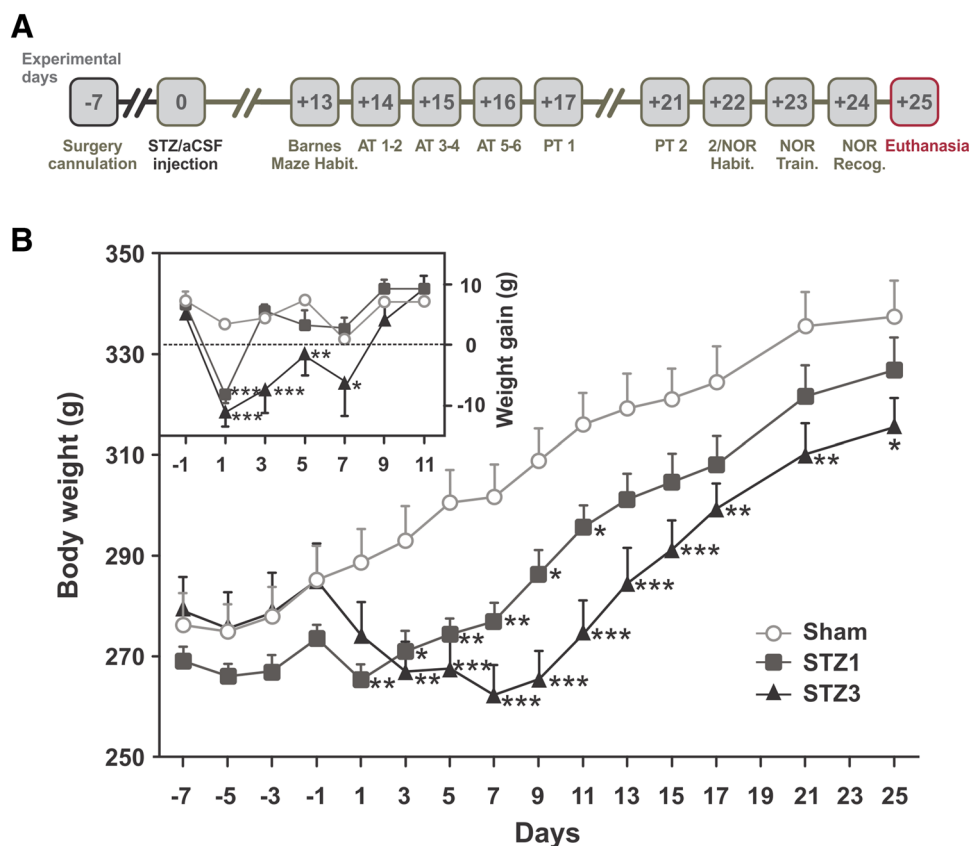


Fig. 1 Experimental design and body weight time course. Stainless-steel guide cannulas were placed in the lateral ventricles on ED -7 . On ED 0, STZ or aCSF was stereotaxically injected. Barnes Maze habituation was performed on ED +13. Subsequently, on ED +14 onward ED +16, all animals were submitted to 120 s AT (2 \times day). PT1 and PT2 were performed on ED +17 and +21, respectively. On ED +22 and +24, NOR test was performed. Finally, on ED +25 rats were sacrificed, and the brains were removed and fixed for morphological analysis (a). Body weight of all rats was registered along

the experiment every 2 days; notice that there was significant weight reduction in the STZ3-treated rats until ED +25 (b). Weight gain from ED -1 until ED +11 (b inset). aCSF artificial cerebrospinal fluid, AT acquisition trial, ED experimental day, Habit. habituation, NOR novel object recognition test, PT probe trial, Recog. recognition session, Train. training session. $N=6$ per group. All data were represented as mean \pm SEM. Comparisons were made versus the corresponding Sham group data point. * $P<0.05$; ** $P<0.01$; *** $P<0.001$

All immunohistochemistry techniques were performed on free-floating sections. For each animal, separate sets of sections were processed using the following antibodies: mouse anti-NeuN antibody (marker of neuronal nuclei; dilution 1:850; Millipore Cat# MAB377.); rabbit anti-Iba1 polyclonal antibody (microglia cells marker, dilution 1:1000; Wako Cat# 016-20001); rabbit anti-GFAP polyclonal antibody (astrocytes marker; dilution 1:1500; DAKO Cat# Z0334). Briefly, after overnight incubation at 4 °C with the primary antibody, sections were incubated with biotinylated goat anti-mouse antibody (dilution 1:300; Vector Laboratories Cat# BA-9200), or a biotinylated goat anti-rabbit antibody (dilution 1:300; Vector Laboratories Cat# BA-1000), as appropriate, for 120 min, rinsed and incubated with avidin–biotin–peroxidase complex (dilution 1:500; Vector Laboratories Cat# PK-6100) for 90 min, and then incubated with 3, 3-diamino benzidine tetrahydrochloride (DAB) or VIP (Vector Laboratories Cat# SK-4600). Sections were counterstained with cresyl violet (Nissl staining) as described elsewhere (Morel et al. 2015). Finally, they were dehydrated and mounted with Vectamount (Vector Laboratories) and used for image analysis.

Image analysis

In each left hemi-hippocampal block, one out of six serial sections was selected to obtain a set of non-contiguous serial sections spanning the dorsal hippocampus. For this task, we used an Olympus BX-51 microscope attached to an Olympus DP70 CCD video camera (Tokyo, Japan).

Within the hippocampus, we focused our analysis on mature neurons, microglial cells, and astrocytes in the SR, whose upper limit is the CA1 pyramidal layer, lower limit is *Stratum Lacunosum Moleculare* (SLM), and lateral limit is the *Stratum Lucidum* (SL) of the dorsal hippocampus (Montgomery 1994).

Volume of the stratum radiatum

To assess the volume of the SR, a stereological approach on rat brain 40 µm-thick coronal sections was carried out. Four Nissl-stained sections were sampled, with a separation of 240 µm along the anterior–posterior axis. Our region of interest was set up as the area delimited by the CA1 pyramidal layer as the upper limit, the SLM as lower limit, and a width of 520 µm as lateral limit, whose midpoint was the inflection point of the pyramidal layer.

Mature neuron analysis

Mature neurons were detected as NeuN immunoreactive (NeuNir) cells. To analyze a possible neurodegeneration, NeuN immunoreactive area was determined. For this

purpose, three sections per animal and three fields per section corresponding to NeuNir neurons in the CA1 pyramidal layer were digitally segmented using *Image Pro Plus v5.1 software* (IPP, Media Cybernetics). For each calculation, background was determined by manually adjusting the system density window as previously described (West and West 1993), until only the NeuNir neurons were selected. For each animal, the sum of immunoreactive areas was multiplied by the section sampling number (NeuNir area × 6). Major nucleus axis was selected as a parameter of cellular changes; this parameter was manually determined using IPP measurement tool in a minimum of 10 nucleuses per section/30 per animal.

Microglial cell analysis

Microglial cells were identified as Iba1 immunoreactive (Iba1ir) cells in the hippocampal SR. The Iba1ir cell number was estimated by a modified version of the optical dissector method (Llorens-Martín et al. 2014). To this end, a random grid consisting of squared probes (area = 5.625 µm²) was superimposed over calibrated images taken at 600× magnification and cells inside the probe area were counted. Iba1ir cells were morphologically classified as Types I, II, III, IV, and V as previously described by as (Diz-Chaves et al. 2013). Types I, II, and III were categorized as non-reactive glia, whereas Types IV and V were taken as reactive glia. *N* = 6 animals per group.

Astroglial cell analysis

Astroglial cell analysis was evaluated in CA1 (SR), DG (dentate hilus, DH), and CA3 (SL). Morphological assessment of GFAP immunoreactive (GFAPir) astrocytes was performed in the SR, DH, and SL. To estimate the area occupied by GFAP cell bodies and processes, GFAPir astrocytes were segmented as described in the “[Mature Neurons Analysis](#)”. For each calculation, background was determined by manually adjusting the system density window until only the GFAPir astrocytes were selected. Three-to-six sections per animal and three fields per section corresponding to GFAPir astrocytes in the SR, DH, and SL were analyzed. For each animal, the sum of immunoreactive areas was divided by the number of sections (GFAPir area/section). The average area of Sham group was considered the 100% GFAPir area and the percentage for the area of each animal was calculated relative to this value.

To study branching complexity, GFAPir astrocytes were submitted to the Sholl analysis (SHOLL DA 1953). In each rat, 25 astrocytes were randomly chosen. Images at high magnification (1000×) were taken throughout representative coronal sections spanning the SR and the SL. Subsequently images were converted to 8-bit monochromatic and analyzed

by the Image J Sholl analysis plugin (<http://imagej.net/Sholl>). This technique consists of superimposing a mask with concentric rings distributed at equal distances (5 μm) centered on a cell soma. The number of process intersections per ring (i), an index of branching complexity, was computed. Afterwards, the total length of the processes was estimated by the sum of the i values for each ring multiplied by 5. The length of the astrocyte processes and their branching complexity at every distance from the soma were averaged, and these output data were used for the statistical analysis between groups.

Western blot analysis

Sample preparation

To obtain protein lysates, the hemi-hippocampi were homogenized with precooled RIPA buffer (150 mM NaCl, 1% Triton X-100, 0.5% sodium deoxycholate, 0.1% SDS, 50 mM Tris-HCl pH 8, and appropriate protease inhibitors, pH 7.4). Finally, protein concentration was measured by Bradford protein assay. Bovine serum albumin (BSA) (0.1–1 mg/ml) was used as a standard. Samples were aliquoted and stored at $-80\text{ }^{\circ}\text{C}$.

Immunoblotting

Equal amounts of protein (75 μg) for every sample were separated by 10% SDS-PAGE and transferred to nitrocellulose membranes (Bio-Rad). The membranes were blocked by incubation in 5% non-fat milk in Tris-buffered saline/Tween-20 (TBS-T) for 1 h at room temperature, and then incubated with primary antibodies against β -Amyloid precursor protein (APP) and β -amyloid peptide ($\text{A}\beta$) (1:200; sc-28365, Santa Cruz Biotechnology), pTau(ser 396) (1:200; sc-101815, Santa Cruz Biotechnology), total Tau (1:150; 5A6, DSHB), and β -Actin (1:1000; sc-47778, Santa Cruz Biotechnology) overnight at $4\text{ }^{\circ}\text{C}$. Then, the membranes were washed with TBS-T and incubated with the corresponding secondary antibody conjugated with horseradish peroxidase (anti-mouse, 1:10000, #115-035-003, Jackson ImmunoResearch Laboratories, Inc., and anti-rabbit, 1:5000, #32460, Thermo Fisher Scientific) for 3 h at room temperature. After washing with TBS-T, membrane visualization was performed with Super Signal West Pico PLUS Chemiluminescent substrate (#34577, Thermo Fisher Scientific) on a Chemidoc Image Station (Bio-Rad, Hercules, CA, USA). Relative optical density of protein bands was analyzed using gel documentation system. Sample loading for APP, $\text{A}\beta$, pTau, and total Tau protein was normalized with Sham group to relative density of the β -Actin band.

Statistical analysis

For BM latency and errors analysis, data from each AT were averaged; these parameters together with body weight were analyzed by two-way repeated measures (RM) ANOVA, considering groups and days factors. In the NOR test, comparisons of total time of exploration during training and recognition sessions on familiar and novel object were examined by paired Student's t test. The stereological data and WB data were analyzed by one-way ANOVA or nonparametric Kruskal–Wallis test. Post hoc tests were used where appropriate. All data were represented as mean \pm SEM and estimated using *Graph Prism Software*. $P < 0.05$ was set as significant.

Results

Weight reduction in STZ-treated rats

As described in the methods section, changes in body weight were assessed in all animals at regular period intervals. Results from Fig. 1b and inset showed that weight of rats treated with STZ1 and STZ3 decreased until ED + 1 and + 7, respectively. After that period, though both STZ groups started to gain weight, there was a significant weight reduction in the STZ3-treated rats as compared with the Sham animals until ED + 23 (two-way ANOVA group factor $F_{(2, 180)} = 68.61$; $P < 0.0001$).

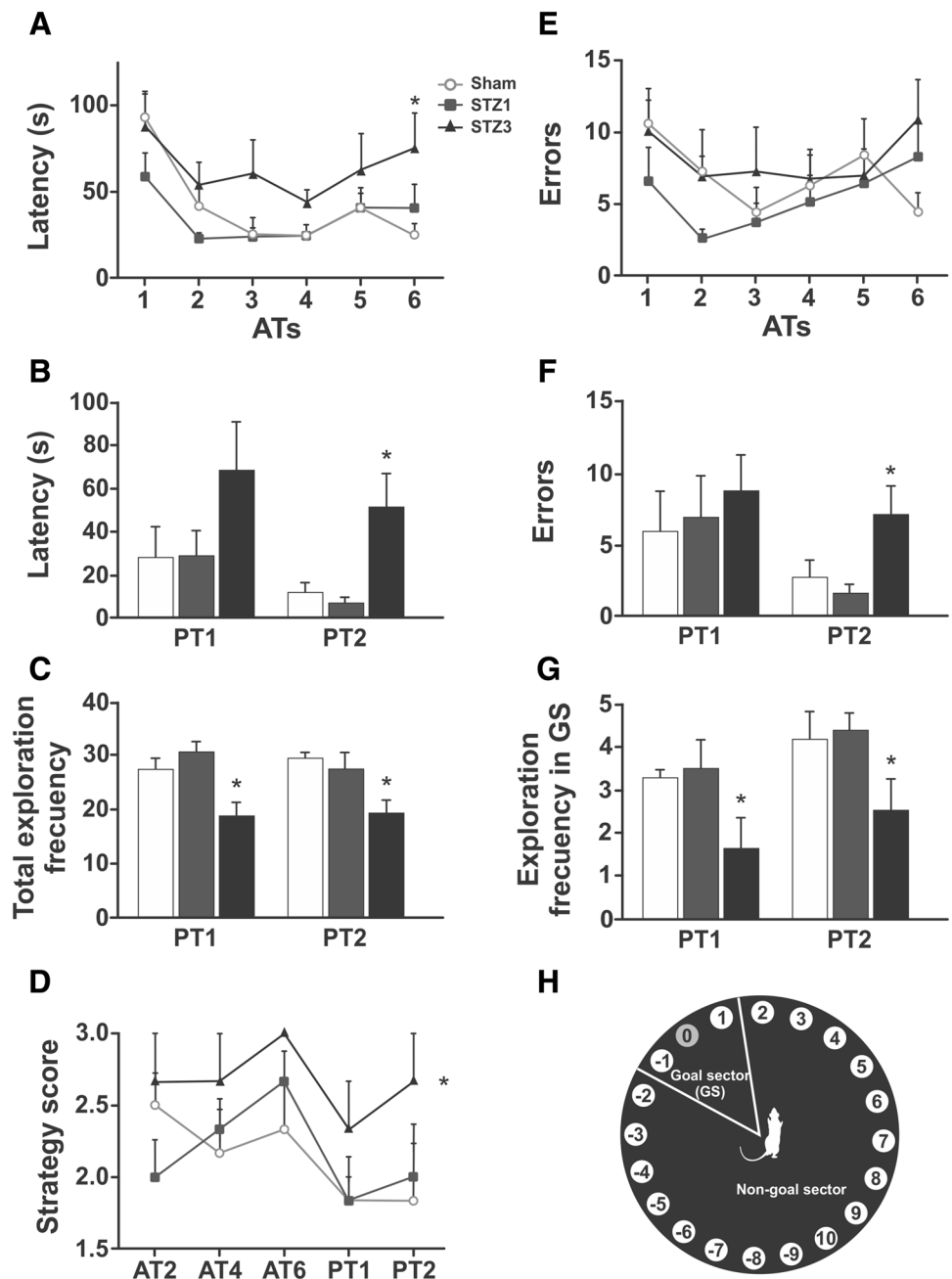
Animal spatial reference learning and memory impairment after icv-STZ administration

Latency to escape box

To assess spatial memory in rats, we used a modified BM test. In the acquisition trials, the latency to reach the escape hole diminished rapidly after Trial 2, in Sham and STZ1 groups, indicating similar learning curves. However, latency remained consistently higher in the STZ3 group and was significantly different in Trial 6 as compared to the Sham group (Fig. 2a; two-way RM ANOVA trial factor $F_{(5, 75)} = 5.988$; $P = 0.0001$; group factor $F_{(2, 15)} = 5.203$; $P = 0.02$).

In the probe trials where the cage was removed, STZ3 group displayed longer latency to reach the target hole for the first time in both PT1 (1 day after ATs) and PT2 (5 days after ATs); this increase was significant in PT2 (Fig. 2b; one-way ANOVA group factor $F_{(2, 15)} = 5.887$; $P = 0.01$), whereas it was only a trend in PT1 (Fig. 2b; one-way ANOVA group factor $F_{(2, 15)} = 1.803$; $P = 0.2$).

Fig. 2 STZ effect on behavioral performance in the Barnes maze test. Latency to the escape box in ATs (a) and PTs (b); latency remained consistently higher in the STZ3 group in ATs and PTs. Numbers of errors in ATs (e) and PTs (f) in the BM; in STZ3 group, errors increased at Trial 6 and PT2. Total exploration frequency (c) and exploration frequency in GS (g) in PT1 and PT2; total and GS exploration frequency in STZ3 animals versus Sham were significantly lower in both PTs. Search strategy scores (d); STZ3 group showed a significant increase in strategy scores; Schematic representation of the maze from above, containing 20 holes around the periphery (h). GS goal sector; PT probe trial. All data were represented as mean \pm SEM. $N=6$ per group. Comparisons were made versus the corresponding Sham group data point. $*P < 0.05$



Errors to escape box

During training sessions, the number of errors fell sharply in Sham and STZ1 animals, indicating similar learning curves. Nevertheless, in STZ3 group, the number of errors declined slightly until reaching a plateau at Trials 2–5 and finally increased at Trial 6 (Fig. 2e; two-way RM ANOVA trial factor $F_{(5, 75)} = 1.415$; $P = 0.2$; group factor $F_{(2, 15)} = 3.387$; $P = 0.06$).

In probe trial sessions, this parameter has not shown difference among the three groups in PT1 (Fig. 2f; one-way ANOVA group factor $F_{(2, 15)} = 0.2714$; $P = 0.77$). However,

STZ3 rats showed an increased in the number of errors committed to reach the target hole as compared to Sham and STZ1 rats in PT2 (Fig. 2f; one-way ANOVA group factor $F_{(2, 15)} = 7.369$; $P = 0.006$).

Total exploration frequency

A significant decrease in total exploration frequency, i.e., the sum of explorations number for each hole of the maze, was observed in STZ3 animals in both PT1 and PT2 sessions (Fig. 2c; one-way ANOVA group factor $F_{(2, 15)} = 7.417$;

$P=0.0058$ and $F_{(2,15)}=5.101$; $P=0.0204$ for PT1 and PT2, respectively).

Goal sector exploration frequency

Goal sector (GS) exploration frequency, i.e. the mean number of explorations in the vicinity of the target hole, was considerably lower in STZ3 rats in both PTs (Fig. 2g; one-way ANOVA Group factor $F_{(2,15)}=4.471$; $P=0.03$ and $F_{(2,15)}=4.006$; $P=0.04$ for PT1 and PT2, respectively), corroborating an impairment in the spatial memory. Otherwise, the exploration frequency for the non-goal sector (NGS) was less affected by STZ administration (data not shown).

Search path

The results of search strategies are shown in Fig. 2d. Sham and STZ1 animals showed similar strategy scores. Compared with the Sham group, STZ3 group had a significantly higher strategy scores, displaying an impaired performance [$F_{(2,15)}=5.356$, $P=0.0176$], and also a higher percentage of random strategy together with lower percentage of spatial strategy (data not shown).

Impairment of animal performance in novel object recognition test after icv-STZ administration

On day 23 following icv-STZ infusion, in the training session involving two identical objects (FO1 and FO2), all the rats took similar time for object exploration (Fig. 3a). On day 24, in the recognition phase (Fig. 3b), when animals were exposed to a familiar (FO1) and a novel object (NO), Sham group showed a significant discrimination between objects (paired t test, $P<0.05$). In addition, STZ1 group spent more time exploring the novel object (paired t test, $P<0.05$). However, STZ3 rats showed an impairment in recognition

memory; they were unable to discriminate between familiar and novel objects and spend almost equal time to explore both of them.

Morphological changes in the rat dorsal hippocampus after icv-STZ administration

Hippocampus volume analysis

SR volume showed a significant decrease between STZ3 and Sham groups (Fig. 4d; one-way ANOVA group factor $F_{(2,13)}=5.377$; $P=0.0235$); no significant differences were found between STZ1 and Sham groups.

Mature neuron analysis

To determine whether behavioral alteration was associated with morphological changes in the brain, NeuNir mature neurons were analyzed in the rat dorsal hippocampus. NeuNir area in the CA1 of the *Stratum Pyramidale* was used as neuron loss index. In this instance, an abrupt reduction of about 26% of CA1 layer was observed in STZ3 animals versus Sham group (Fig. 4e; one-way ANOVA group factor $F_{(2,13)}=3.807$; $P=0.05$). In addition, major nucleus axis was employed as parameter of cellular morphology alterations. In this regard, STZ3 animals showed a sharp cell reduction of about 16% (Fig. 4f; one-way ANOVA group factor $F_{(2,12)}=9.443$; $P=0.0034$) as compared with Sham rats. However, STZ1 rats showed no significant differences compared to Sham rats in either of the two parameters.

Microglial cell analysis

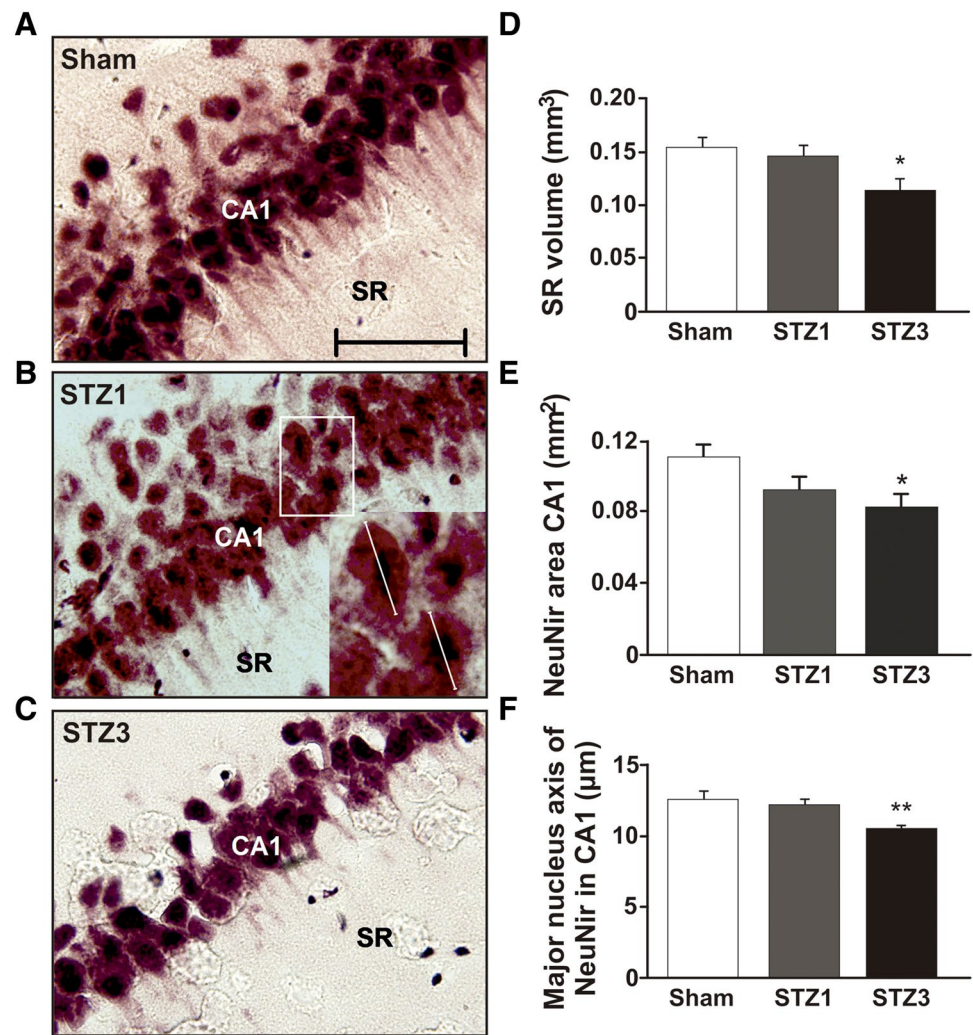
Ibalir microglial cells were counted and classified as non-reactive and reactive in the hippocampal SR. There were no significant differences in the number of non-reactive



Fig. 3 STZ effect on behavioral performance in the novel object recognition test. Time spent exploring two identical objects in the training session (a): rats of the three groups spent similar time for familiar objects (FO1 and FO2) exploration. Time spent exploring the novel

object in the recognition session (b): Sham and STZ1 rats showed preference to the novel object (NO) exploration. All data were represented as mean \pm SEM. $N=6$ per group. Comparisons were made versus the exploration time of FO in each group. * $P<0.05$

Fig. 4 Morphometric analysis of *Stratum Radiatum* (SR) volume and mature neuron nucleus size in CA1 pyramidal cells. Coronal sections of the SR in representative animals of each group showing NeuN immunoreactive (NeuNir) cells (a–c). Quantification of the SR volume (d) showing a hippocampal atrophy process only in the STZ3-treated group. A reduction in NeuNir area in the hippocampal CA1 pyramidal layer (e) was observed in STZ3 group. Major cell body axis of NeuNir cells in CA1 (f); notice that the neuron nucleus size decreased in STZ3 rats. Scale bar 50 μm . $N=6$ per group. All data were represented as mean \pm SEM. Comparisons were made versus the Sham group data point. * $P<0.05$; ** $P<0.01$



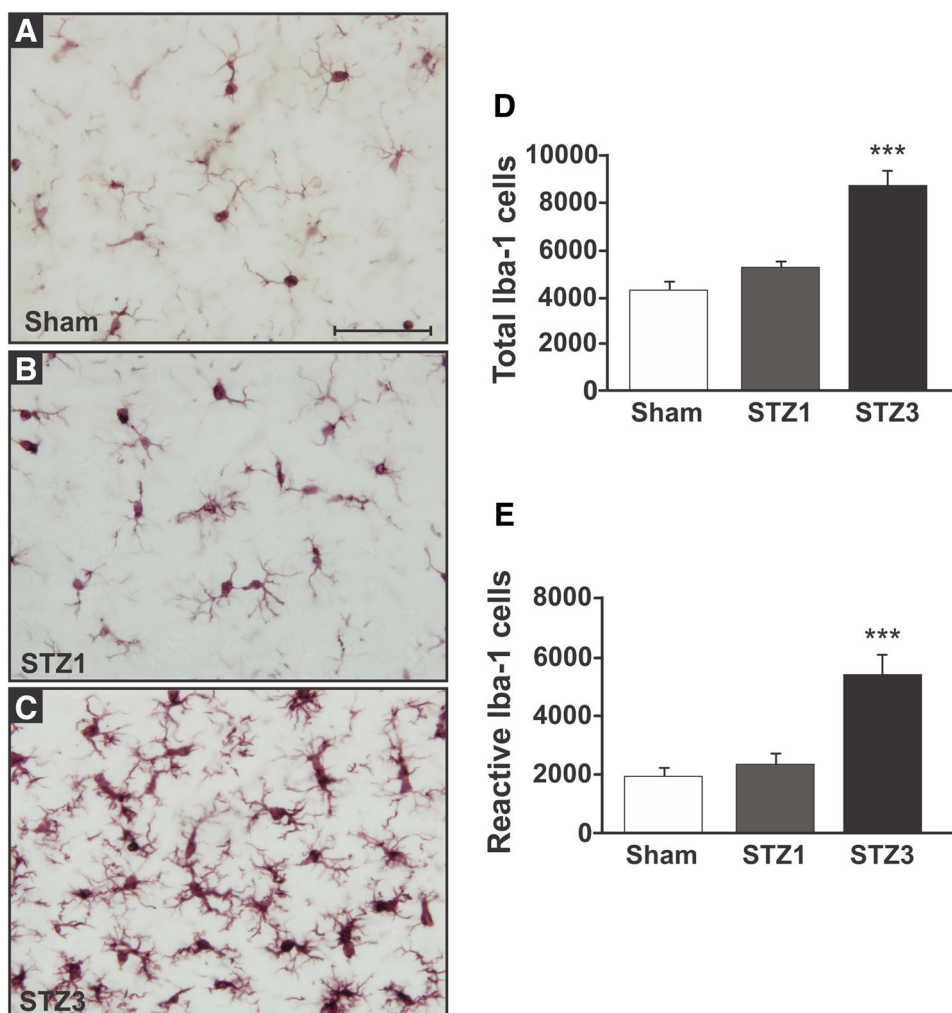
microglial cells for the three experimental groups (data not shown). In addition, total (non-reactive plus reactive) and reactive number of microglial cells in STZ1 rats were similar to Sham rats (Fig. 5d, e, respectively). However, a notable increase in the total (Fig. 5d; one-way ANOVA group factor $F_{(2, 15)} = 26.94$; $P < 0.0001$) and in the number of reactive microglial cells (Fig. 5e; one-way ANOVA group factor $F_{(2, 15)} = 14.72$; $P = 0.0003$) was observed in STZ3 group versus Sham group.

Astroglial cell analysis

The percentage of GFAPir (astroglial) area was evaluated in the hippocampal SR, DH, and SL (Fig. 6a–i). STZ3 group displayed a tendency to increase the GFAPir area in SR and DH, in contrast with Sham rats (Fig. 6j–k. SR: nonparametric Kruskal–Wallis test; $P = 0.190$. DH: $F_{(2, 15)} = 1.205$, $P = 0.3272$). On the other hand, SL GFAPir area showed a significant increase between STZ3 and Sham groups (Fig. 6l; one-way ANOVA group factor $F_{(2, 15)} = 5.204$;

$P = 0.0192$); no significant differences were found between STZ1 and Sham groups for this parameter. No significant differences were found in the GFAPir cell number of SR, DH, and SL for the three experimental groups (data not shown. SR: $F_{(2, 15)} = 2.498$; $P = 0.1158$. SL: $F_{(2, 15)} = 1.710$; $P = 0.2143$. DH: $F_{(2, 15)} = 2.601$; $P = 0.1072$). In addition, an important fall in SR branching complexity was observed at 10–20 μm and 10–25 μm from the cell soma for STZ1 and STZ3 animals, respectively, versus Sham animals (Fig. 7b; one-way ANOVA group factor $F_{(2, 14)} = 11.32$, $P = 0.001$; $F_{(2, 14)} = 13.87$, $P = 0.0005$; $F_{(2, 14)} = 7.584$, $P = 0.006$ and $F_{(2, 14)} = 4.182$, $P = 0.038$ for 10, 15, 20, and 25 μm , respectively). Similarly, a reduction in SL branching complexity was observed at 30–35 μm and 15–25 μm from the cell soma for STZ1 and STZ3 animals, respectively, versus Sham animals (Fig. 7c; one-way ANOVA group factor $F_{(2, 15)} = 5.974$, $P = 0.0124$; $F_{(2, 15)} = 2.704$, $P = 0.0993$; $F_{(2, 15)} = 4.386$, $P = 0.0316$; $F_{(2, 15)} = 5.471$, $P = 0.0164$; $F_{(2, 15)} = 4.485$, $P = 0.0297$ for 15, 20, 25, 30, and 35 μm , respectively).

Fig. 5 Iba1 immunoreactive microglial cells (Iba1ir) in the hippocampal *Stratum Radiatum* (SR). Magnified microphotography (600 \times) of the SR in representative animals of each group showing Iba1ir cells (a–c). Quantification of total (d) and reactive (e) Iba1ir cell number showing an increase in microglial cell number in STZ3 rats. Scale bar 200 μ m. $N=6$ per group. All data were represented as mean \pm SEM. Comparisons were made versus the Sham group data point. *** $P < 0.001$



Consistently, a reduction in the mean length of astrocyte processes was observed in STZ-treated compared to Sham rats in SR (Fig. 7c; one-way ANOVA group factor $F_{(2, 15)} = 6.473$; $P = 0.0094$) and in SL (Fig. 7e; one-way ANOVA group factor $F_{(2, 15)} = 5.425$, $P = 0.0169$).

Furthermore, the number of branches emerging from the cell soma was significantly affected by icv-STZ in SR, and being more pronounced in STZ3 than in STZ1 group, as compared with Sham group (data not shown; one-way ANOVA group factor $F_{(2, 15)} = 6.781$; $P = 0.008$). In contrast, this parameter was not significantly affected in SL (data not shown; one-way ANOVA group factor $F_{(2, 15)} = 1.645$; $P = 0.2261$). This result indicates that entire arbors were lost in CA1, while only the distal branches were lost in CA3.

APP, A β , and pTau/Tau protein levels after icv-STZ administration

Pathological APP cleavage and the accumulation of A β are hallmarks of AD and a preferred criterion for the validation of experimental models of AD. To explore the effect of

STZ on the production of A β in the hippocampus, we determined the protein levels of APP and A β by WB. Although there were no significant differences in APP protein levels for the three experimental groups (Fig. 8a, b; one-way ANOVA group factor $F_{(2, 15)} = 1.553$; $P = 0.2439$), icv-STZ induces a trend to increase APP protein levels. WB analysis revealed an increase in A β protein levels in the STZ3 group (Fig. 8a, c; one-way ANOVA Group factor $F_{(2, 15)} = 3.724$; $P = 0.0486$) as compared to the Sham group. No significant differences in A β protein levels were found between STZ1 and Sham groups (Fig. 8c).

Intracellular neurofibrillary tangles containing hyperphosphorylated tau protein are a major neuropathological feature of AD. We studied the accumulation of hyperphosphorylated tau in the hippocampus of icv-STZ rats by assessing the ratio of pTau(ser396)/total Tau protein levels. WB analysis revealed a significant increase in pTau(ser396) protein levels in the STZ3 group (one-way ANOVA Group factor $F_{(2, 15)} = 4.286$; $P = 0.0337$) as compared to the Sham group (data not shown). In addition, there was a significant increase in pTau(ser396)/total Tau ratio in the STZ3 group as

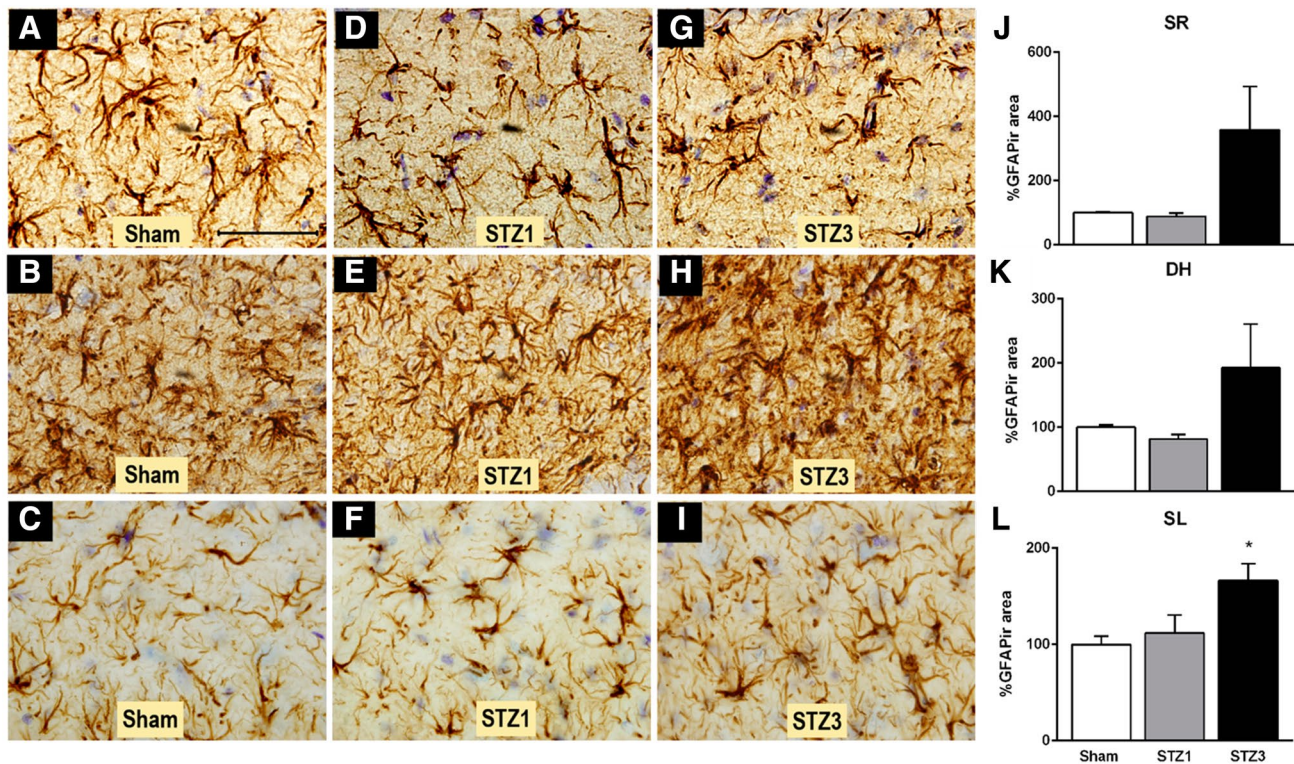


Fig. 6 GFAP immunoreactive astrocytes in the dorsal hippocampus. Coronal sections of representative animals of each group showing GFAPir cells (1000 \times). **a–c**, **d–f**, **g–i** panels represent magnified views of SR, DH, and SL regions, respectively. Bar plot shows an increase

in GFAPir area in the STZ3 rats in SR (**j**), DH (**k**), and SL (**l**). Scale bar 50 μ m (panels **a–i**). $N=6$ per group. All data were represented as mean \pm SEM. Comparisons were made versus the Sham group data point. * $P < 0.05$

compared to the Sham group (Fig. 8a, d; one-way ANOVA group factor $F_{(2, 15)} = 4.559$; $P = 0.0284$). However, no significant differences in pTau(ser396) protein levels (data not shown) and in pTau/Tau ratio were found between STZ1 and Sham groups. There were no significant differences in total Tau protein levels for the three experimental groups (one-way ANOVA Group factor $F_{(2, 15)} = 0.2628$; $P = 0.7723$) (data not shown).

Discussion

icv-STZ model has been proposed as a representative model of SAD (Lannert and Hoyer 1998; Salkovic-Petrisic and Hoyer 2007, Mayeret al. 1990), since it induces biochemical, structural, and cognitive effects together with an insulin-resistant brain state in a standardized and reproducible manner in all investigated species (rats, mice, and monkeys). Besides, icv-STZ model demonstrates several advantages over the transgenic mice AD models (Salkovic-Petrisic et al. 2013).

It was previously shown that icv-STZ injection produces a marked initial loss of body weight in rats (Shoham et al. 2003, Pathan et al. 2006). In agreement with these findings,

our study also evidenced that icv-STZ treatment caused a significant reduction in body weight. STZ3 group showed the lowest body weight through the whole experiment. Indeed, after icv injection, Sham rats gained body weight, whereas icv-STZ rats decreased their body weight until ED + 1 and + 7 in STZ1 and STZ3 groups, respectively. Other report showed an initial weight loss and hypophagia in icv-STZ-treated rats (Majkutewicz et al. 2016b). This work also showed that these rats present an enlargement of the third ventricle and the ventricular space, resulting in a loss of ependymal cells and damage to hypothalamic periventricular myelin and shrinkage of fornix, respectively. We observe similar enlargement of ventricles of STZ3 rats (data not shown). This could explain the temporally weight loss seen after icv injection of STZ and even could affect the animals cognition.

A growing body of scientific evidence demonstrates impaired learning and memory in icv-STZ-treated rats assessed in MWM, at different STZ doses (0.5–6 mg/kg) and at several time points after injection (Grünblatt et al. 2007; Salkovic-Petrisic et al. 2015, Rajasekar et al. 2017). In line with this, learning parameters show that icv-STZ 3 mg/kg causes a progressive decrease in latency time together with an increasing trend of errors in the BM. Compared

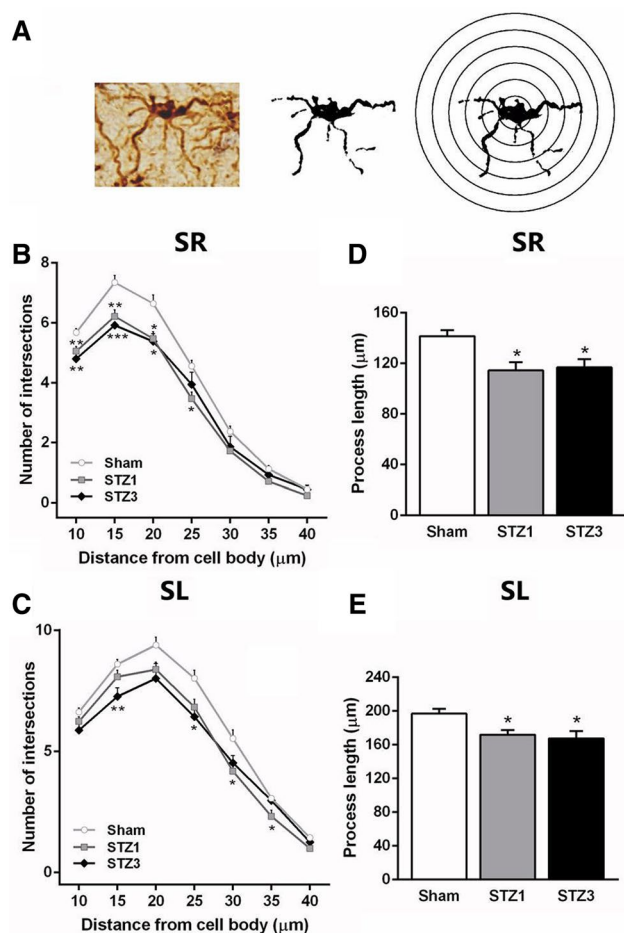


Fig. 7 Sholl analysis of GFAP immunoreactive astrocytes in the dorsal hippocampus. **a** Micrograph of a single astrocyte and the result of superimposing a mask with concentric rings distributed at equal distances (5 μm) and centered on the GFAPir soma of the astrocyte silhouette. The number of process intersections i per ring was computed as branching complexity in SR (**b**) and SL (**c**); an important fall in branching complexity was observed in STZ-treated animals. **d**, **e** Average length of astrocyte processes in SR and SL, respectively. The length of the processes was estimated by the sum of the i values for each ring multiplied by 5. A reduction in the mean length of astrocyte processes was observed in STZ-treated rats. $N=25$ astrocytes for each rat. $N=6$ per group. All data were represented as mean \pm SEM. Comparisons were made versus the Sham group data point. * $P < 0.05$; ** $P < 0.01$; *** $P < 0.001$

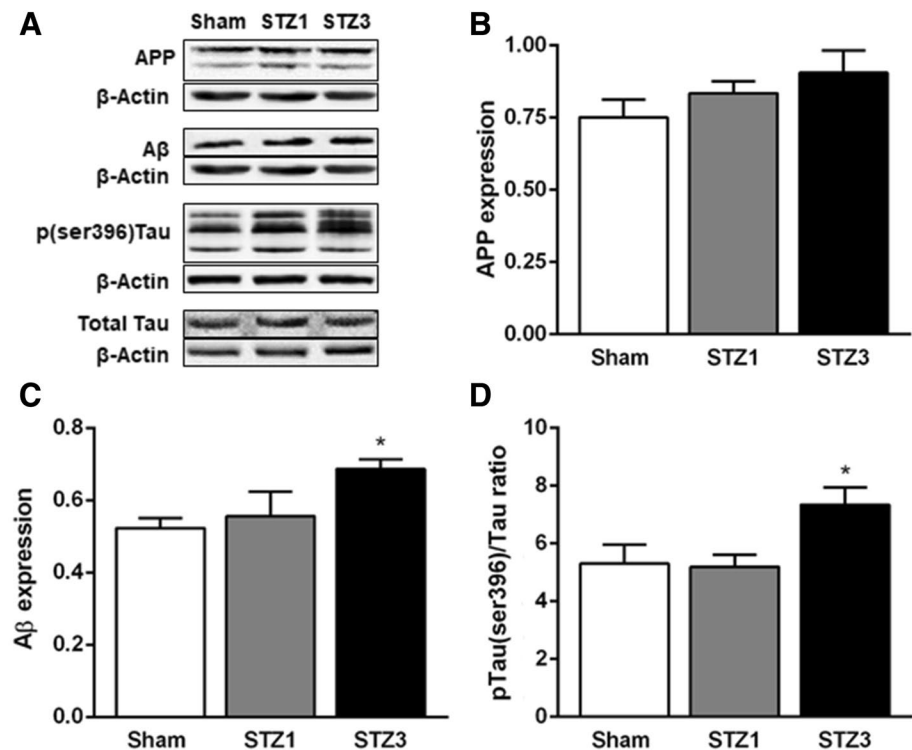
with more extensive BM protocols (Rosenfeld and Ferguson 2014, Gawel et al. 2016; de la Tremblaye et al. 2017), in this work, the number of acquisition sessions (six AT in 3 days) were abbreviated but sufficient to detect impaired learning efficiency. In addition, recent studies of our group demonstrated the usefulness of this BM protocol to evaluate spatial memory impairment in old rats (Morel et al. 2015). The previous BM works identified that intact rats performance was equivalent in the first two PTs, but then they became habituated and cannot be further tested (Uriarte et al. 2017). In the present study, short- and long-term spatial memory

retention was evaluated, 1 and 5 days after the last AT in PT1 and PT2, respectively.

In these two instances, a significant fall in GS exploration frequency was observed, expressed as the mean number of explorations in the vicinity of the target hole, for both icv-STZ doses. At least two components contribute to the magnitude of GS exploration frequency, namely spatial memory retention and target-seeking activity. The latter depends mainly on the motivation to search for the escape hole. There are some reports suggesting that mice and rats treated with icv-STZ have motivational difficulties (Rostami et al. 2017, Shayan Amiri et al. 2017). In this work, motivational behavior was evaluated as the total exploration frequency and our results show a decline in STZ3-injected animals but not in STZ1 group. Therefore, STZ3 rats exhibit a loss of motivation and impaired short and long-term spatial memory retention. Moreover, memory performance was evaluated through escape hole latency time and number of errors (explorations of holes different from the escape one). Our data indicate that memory disruption by icv-STZ3 is stronger in long-term retention, since animals take significantly longer time to find the escape hole and are more erratic. This deficit was not observed with STZ 1 mg/kg dose. These results are in accordance with the previous studies (Rostami et al. 2017, Mehla et al. 2013), showing that the icv-STZ impairment of reference memory in animals is dose-dependent. In addition, the more frequent use of random search strategy to locate the escape hole may underlie the poor performance of STZ3 rats during acquisition training, as they were worse at finding the escape hole than controls. It is worth noting that, before the initiation of cognitive evaluation, we assessed motor performance and no significant differences were found between the groups (data not shown), in accordance with the previous studies (Ozkay et al. 2012, Saxena et al. 2011; Bokare et al. 2018). Overall, these results replicated learning deficits in the Morris water maze (Gao et al. 2014, Majkutewicz et al. 2016b; Salkovic-Petrisic et al. 2015) and suggest that STZ3 dose can result in spatial learning deficits on the Barnes maze.

Novel object recognition is related to hippocampal memory (Clark et al. 2000). Therefore, an alteration in Barnes Maze would predict NOR test impairment. Indeed, our data showed that STZ 3 mg/kg injection induced a deficit in long-term object recognition memory (24 h after the training session). This finding is consistent with a previous study in which long-term object recognition memory deficits in rats were observed 3 weeks after icv-STZ3 (Kheradmand et al. 2018). Although there are no changes in the STZ1 group, we suggest a longer time after STZ1 injection would reveal a significant object recognition memory impairment. Other studies reported that damaging effects of STZ 1 mg/kg dose are mainly progressive (Grünblatt et al. 2007; Shoham et al. 2007; Knezovic et al. 2015; Kraska et al. 2012). Shoham

Fig. 8 STZ effect on protein levels in the rat hippocampus. Representative images of APP, A β , pTau(ser396), total Tau, and β -Actin protein levels in hippocampus of rats of each experimental group (a). Quantification of protein levels of APP (b), A β (c), and pTau(ser396)/total Tau ratio (d), normalized to Sham group to relative density of β -Actin. STZ3 induced a significant increase in A β and pTau(ser396)/total Tau ratio protein levels. $N=6$ per group. All data are represented as mean \pm SEM. Comparisons were made versus the Sham group data point. $*P < 0.05$



et al. (2007) informed impaired long-term object recognition memory 4 weeks after icv-STZ injection (Shoham et al. 2007). In accordance, Rostami et al. (2017) described a short-term object recognition memory deficit (1 h after the training session) 4, 10 and 14 weeks after icv-STZ injection (Rostami et al. 2017). Together, these data suggest distinct late onset in the STZ-induced object recognition memory impairment.

Human AD studies show that a reduction in hippocampal volume is correlated with global cognitive function and memory performance (Su et al. 2018, Elgh et al. 2006, Stoub et al. 2006). In our study, administration of icv-STZ3 resulted in SR volume reduction of the dorsal hippocampus. This hippocampal subfield area is one of the most affected in AD and was proposed as a potential early biomarker for detecting AD at the mild cognitive impairment (MCI) stage (Su et al. 2018). In accordance another study proposed that both volume and neuronal loss in CA1 of the hippocampal formation, are early hallmarks of Alzheimer's disease, and are strongly correlated with cognitive status (Bobinski et al. 1998). In this respect, we observed a significant reduction of hippocampal CA1 pyramidal layer in STZ3 rats and a partial reduction in STZ1 group. It was previously reported that NeuN immunostaining correlates with neuronal death (Davoli et al. 2002); interestingly, an increased number of apoptotic cells in the icv-STZ SAD model were also reported (Hashemi-Firouzi et al. 2017). Moreover, it was observed that STZ induced neurodegeneration in the hippocampus, particularly in the CA1 area (Majkutewicz et al. 2016a, b).

Based on these data, we suggest that the decrease in NeuN immunostaining in STZ3 group is associated with neuronal death in the dorsal hippocampus. In addition, it is noticed a severe reduction of cell bodies of neurons in STZ3 rats. In fact, remarkable changes in the neuron morphology were found, such as atrophy and shrinkage. However, the hippocampal CA1 cells structure of STZ1 group was uniform and similar to that of the Sham group. Thus, icv-STZ3 rat model shows consistent structural CA1 and SR atrophy that contributes to memory decline. By contrast, other rodent models of AD show neither volume changes (Klementiev et al. 2007) nor neuronal loss in an equivalent period to that evaluated by us (Wirhns and Bayer 2010).

Neuroinflammation, as reflected by astrogliosis and microglial activation, is another hallmark that is thought to contribute to AD pathogenesis (McGeer and McGeer 2003). Reactive gliosis of AD histopathology reflects the abnormal morphology of astrocytes and microglia.

Microglia is resident phagocytes of the CNS that dynamically survey the environment, playing crucial roles in brain tissue maintenance, injury response, and pathogen defense (Nayak et al. 2014, Colonna and Butovsky 2017). Microglia have emerged as crucial players in the pathogenesis of SAD and there is considerable evidence that microglia are responsible for neuronal damage in this pathology (Hansen et al. 2017). Our results are consistent with these alterations and demonstrate that there is a significant proliferation of reactive microglia in the hippocampus in STZ3-SAD model. Prolonged microglial activation leads to pro-inflammatory

cytokines' release that exacerbates neuroinflammation, contributing to neuronal loss and cognitive function impairment (Streit et al. 2004, Perry et al. 2010; Jiang et al. 2012). Thus, understanding the signals that trigger microglia to prune vulnerable circuits could provide important insights into neurodegenerative diseases and shed light on novel therapeutic targets. Given the diverse and complex activity of microglia in healthy and diseased brain, there is a critical need for new biomarkers that may relate specific microglial functional states to disease progression and pathobiology.

Astrocytes are responsible for maintaining homeostasis in the CNS. In AD, both reactivity and atrophic changes in astrocytes were reported [see an extend revision in Rodríguez-Arellano et al. (2016)]. In STZ3-SAD model, an increased astrocytes number in the hippocampus and other brain regions was observed (Rostami et al. 2017, Kraska et al. 2012; Dos Santos et al. 2018). An increased GFAP immunoreactivity has also been described at different times post icv-STZ in rats (Bassani et al. 2017, Knezovic et al. 2017, Shi et al. 2017). In contrast, other works reported no significant change in GFAP content in the hippocampus of rats submitted to icv-STZ injection (Rodrigues et al. 2010; Biasibetti et al. 2013).

To elucidate these controversial findings in the icv-STZ model, we analyzed three hippocampal regions known to be involved in learning and spatial memory: SR, DG, and SL. Our results demonstrate that icv-STZ tends to increase GFAPir area in the SR and DH; in particular, high doses incremented more than 100% of GFAPir area. This increment was significant in SL region. Due to this augmentation, we can hypothesize that cells are hypertrophied. The previous reports demonstrated that AD patients display GFAP hyper-reactivity with signs of cellular hypertrophy in the hippocampus (Vijayan et al. 1991) and in the cerebral cortex (Colombo et al. 2002). On the other hand, as our three experimental groups showed similar GFAPir cell number in hippocampal regions analyzed, STZ injection does not seem to have modified this parameter. However, since hippocampal atrophy was observed in STZ3 rats, it can be inferred that SR, DH, and SL cell ratio is modified, i.e., the same GFAPir cell number occupies a smaller brain parenchyma volume in STZ3 brains.

We also performed detailed morphometric analyses in SR and SL astrocytes of icv-STZ rats to evaluate their complexity by the Sholl analysis. This is the first work to analyze the effect of two doses of icv-STZ on astrocytes morphology. On a cellular level, icv-STZ promotes a decrease in astrocyte complexity, as reflected by processes' length reduction, and less branching complexity in both hippocampal regions, and decrease number of main processes in SR, thus resulting in decreased arborization of STZ1 and STZ3 rats compared to Sham rats. Taking into consideration all parameters, astrocyte complexity was the unique significantly affected one

for low doses of icv-STZ. Previously, a decrease in astrocytes complexity in the post-mortem brains of dementia patients was reported (Senitz et al. 1995). Consequently, it is then conceivable to speculate that astrocyte vulnerability accompanies the onset of AD. Besides, we assume that these impaired astrocytes fail to provide adequate neuron-glia signaling inducing synaptic loss, what is, indeed, observed in the early stages of AD and may be a driving factor in the development of cognitive deficits.

The accumulation of A β and abnormal phosphorylated tau protein is suggested to contribute to hippocampal atrophy in AD brain (Dhikav and Anand 2011, Irvine et al. 2008). Regarding this, in the icv-STZ model, an increase in amyloidogenesis (Salkovic-Petrisic et al. 2011) and that in tau hyperphosphorylation (Grünblatt et al. 2007) have been observed. In line with these studies, we have found an increase in A β and pTau(ser396) protein levels, a trend to increase for APP, and no changes in total Tau protein levels in the hippocampus of STZ3 group. However, no significant differences in the levels of these proteins were found in the STZ1 group. It was reported that Tau hyperphosphorylation at ser396 is responsible for the functional loss of Tau-mediated tubulin polymerization (Evans et al. 2000). Thus, we confirmed the accumulation of A β and tauopathy in the hippocampus of icv-STZ rat model, 25 days after STZ administration.

Conclusion

In the present study, we highlighted the difference of lesions induced by low and high doses of STZ in a short-term study. Our evidence revealed that a single high STZ dose (3 mg/kg) administration into the lateral ventricles induces severe spatial and recognition memory impairment together with morphological and biochemical changes in the rat dorsal hippocampus, which were observed 25 days after the treatment. At low doses (1 mg/kg), the icv-STZ did not significantly affect animal cognition and induced moderate or not detected lesions. Moreover, both doses induced a reduction in astrocyte-branching complexity. Consequently, we suggest that the mechanisms induced at the two doses might be different, resulting in an acute toxic effect triggered by the high dose or a partial toxic effect caused by the lower dose.

In summary, the BM was an alternative test to evaluate the cognitive performance in this SAD model. In addition, we propose STZ3 as the dose of choice to evaluate the SAD symptoms, to study possible therapies, and to detect potential early biomarkers in the rat brain. On the other side, we propose STZ1 as the adequate dose to evaluate the early stages of AD and to study the role of astrocytes in this disease.

Acknowledgements The authors thank to Dr. Joaquín Pardo, Ms. Natalia Scelcio, and Ms. Romina Becerra for technical assistance, Ms. Rosana del Cid for English edition, Mr. Mario R. Ramos for graphic designs, and Mr. Oscar Vercellini, Araceli Bigres, and Juan Manuel Lofeudo for animal care assistance. PCR and GRM are career researchers of the Argentine Research Council (CONICET). MFZV, JLH, and EFL are recipients of CONICET doctoral fellowships. LST is a recipient of National Interuniversity Council (CIN) fellowship. This work was supported by grants #PICT12-2461 and #PICT15-1998 from the Argentine Agency for the Promotion of Science and Technology and grant PIP0570 from CONICET to PCR.

Compliance with ethical standards

Conflict of interest There are no conflicts of interest concerning any of the authors.

References

- Barnes CA (1979) Memory deficits associated with senescence: a neurophysiological and behavioral study in the rat. *J Comp Physiol Psychol* 93(1):74–104
- Bassani TB, Turnes JM, Moura ELR, Bonato JM, Cópola-Segovia V, Zanata SM, Oliveira RMMW, Vital MABF (2017) Effects of curcumin on short-term spatial and recognition memory, adult neurogenesis and neuroinflammation in a streptozotocin-induced rat model of dementia of Alzheimer's type. *Behav Brain Res* 335:41–54
- Biasibetti R, Tramontina AC, Costa AP, Dutra MF, Quincozes-Santos A, Nardin P, Bernardi CL, Wartchow KM, Lunardi PS, Gonçalves CA (2013) Green tea (–)epigallocatechin-3-gallate reverses oxidative stress and reduces acetylcholinesterase activity in a streptozotocin-induced model of dementia. *Behav Brain Res* 236(1):186–193
- Blokland A, Jolles J (1993) Spatial learning deficit and reduced hippocampal ChAT activity in rats after an ICV injection of streptozotocin. *Pharmacol Biochem Behav* 44(2):491–494
- Bobinski M, de Leon MJ, Tarnawski M, Wegiel J, Reisberg B, Miller DC, Wisniewski HM (1998) Neuronal and volume loss in CA1 of the hippocampal formation uniquely predicts duration and severity of Alzheimer disease. *Brain Res* 805(1–2):267–9
- Bokare AM, Bhonde M, Goel R, Nayak Y (2018) 5-HT₆ receptor agonist and antagonist modulates ICV-STZ-induced memory impairment in rats. *Psychopharmacology* 235(5):1557–1570
- Broadbent NJ, Gaskin S, Squire LR, Clark RE (2009) Object recognition memory and the rodent hippocampus. *Learn Mem* 17(1):5–11
- Clark RE, Zola SM, Squire LR (2000) Impaired recognition memory in rats after damage to the hippocampus. *J Neurosci* 20(23):8853–8860
- Colombo JA, Quinn B, Puissant V (2002) Disruption of astroglial interlaminar processes in Alzheimer's disease. *Brain Res Bull* 58(2):235–242
- Colonna M, Butovsky O. Microglia function in the central nervous system during health and neurodegeneration. *Annu Rev Immunol*. 2017 Apr 26;35:441–468
- Davoli MA, Fourtounis J, Tam J, Xanthoudakis S, Nicholson D, Robertson GS, Ng GY, Xu D (2002) Immunohistochemical and biochemical assessment of caspase-3 activation and DNA fragmentation following transient focal ischemia in the rat. *Neuroscience* 115(1):125–136
- de la Monte SM, Tong M, Lester-Coll N, Plater M Jr, Wands JR (2006) Therapeutic rescue of neurodegeneration in experimental type 3 diabetes: relevance to Alzheimer's disease. *J Alzheimers Dis* 10(1):89–109
- de la Tremblaye PB, Benoit SM, Schock S, Plamondon H (2017) CRHR1 exacerbates the glial inflammatory response and alters BDNF/TrkB/pCREB signaling in a rat model of global cerebral ischemia: implications for neuroprotection and cognitive recovery. *Prog Neuropsychopharmacol Biol Psychiatry* 79(Pt B):234–248
- Deshmukh R, Kaundal M, Bansal V, Samardeep (2016) Caffeic acid attenuates oxidative stress, learning and memory deficit in intracerebroventricular streptozotocin induced experimental dementia in rats. *Biomed Pharmacother* 81:56–62
- Dhikav V, Anand K (2011) Potential predictors of hippocampal atrophy in Alzheimer's disease. *Drugs Aging* 28(1):1–11
- Diz-Chaves Y, Astiz M, Bellini MJ, Garcia-Segura LM (2013) Prenatal stress increases the expression of proinflammatory cytokines and exacerbates the inflammatory response to LPS in the hippocampal formation of adult male mice. *Brain Behav Immun* 28:196–206
- Dos Santos JPA, Vizuete A, Hansen F, Biasibetti R, Gonçalves CA (2018) Early and persistent O-GlcNAc protein modification in the streptozotocin model of Alzheimer's disease. *J Alzheimers Dis* 61(1):237–249
- Duelli R, Schröck H, Kuschinsky W, Hoyer S (1994) Intracerebroventricular injection of streptozotocin induces discrete local changes in cerebral glucose utilization in rats. *Int J Dev Neurosci* 12(8):737–743
- Elgh E, Lindqvist Astot A, Fagerlund M, Eriksson S, Olsson T, Näslman B (2006) Cognitive dysfunction, hippocampal atrophy and glucocorticoid feedback in Alzheimer's disease. *Biol Psychiatry* 59(2):155–161
- Evans DB, Rank KB, Bhattacharya K, Thomsen DR, Gurney ME, Sharma SK (2000) Tau phosphorylation at serine 396 and serine 404 by human recombinant tau protein kinase II inhibits tau's ability to promote microtubule assembly. *J Biol Chem* 275(32):24977–24983
- Gao C, Liu Y, Jiang Y, Ding J, Li L (2014) Geniposide ameliorates learning memory deficits, reduces tau phosphorylation and decreases apoptosis via GSK3 β pathway in streptozotocin-induced Alzheimer rat model. *Brain Pathol* 24(3):261–269
- Gawel K, Labuz K, Gibula-Bruzda E, Jenda M, Marszałek-Grabska M, Filarowska J, Silberring J, Kotlinska JH (2016) Cholinesterase inhibitors, donepezil and rivastigmine, attenuate spatial memory and cognitive flexibility impairment induced by acute ethanol in the Barnes maze task in rats. *Naunyn-Schmiedeberg's Arch Pharmacol* 389(10):1059–1071
- Glowinski J, Iversen LL (1966) Regional studies of catecholamines in the rat brain. I. The disposition of [³H]norepinephrine, [³H]dopamine and [³H]dopa in various regions of the brain. *J Neurochem* 13(8):655–669
- Grünblatt E, Salkovic-Petrisic M, Osmanovic J, Riederer P, Hoyer S (2007) Brain insulin system dysfunction in streptozotocin intracerebroventricularly treated rats generates hyperphosphorylated tau protein. *J Neurochem* 101(3):757–770
- Hansen DV, Hanson JE, Sheng M (2017) Microglia in Alzheimer's disease. *J Cell Biol*
- Hashemi-Firouzi N, Komaki A, Soleimani Asl S, Shahidi S (2017) The effects of the 5-HT₇ receptor on hippocampal long-term potentiation and apoptosis in a rat model of Alzheimer's disease. *Brain Res Bull* 135:85–91
- Hellweg R, Nitsch R, Hock C, Jaksch M, Hoyer S (1992) Nerve growth factor and choline acetyltransferase activity levels in the rat brain following experimental impairment of cerebral glucose and energy metabolism. *J Neurosci Res* 31(3):479–486
- Heo JH, Lee SR, Lee ST, Lee KM, Oh JH, Jang DP, Chang KT, Cho ZH (2011) Spatial distribution of glucose hypometabolism induced by intracerebroventricular streptozotocin in monkeys. *J Alzheimers Dis* 25(3):517–523

- Irvine GB, El-Agnaf OM, Shankar GM, Walsh DM (2008) Protein aggregation in the brain: the molecular basis for Alzheimer's and Parkinson's diseases. *Mol Med* 14(7–8):451–464
- Isik AT, Celik T, Ulusoy G, Ongoru O, Elibol B, Doruk H, Bozoglu E, Kayir H, Mas MR, Akman S (2009) Curcumin ameliorates impaired insulin/IGF signalling and memory deficit in a streptozotocin-treated rat model. *Age (Dordr)* 31(1):39–49
- Jiang T, Yu JT, Tan L (2012) Novel disease-modifying therapies for Alzheimer's disease. *J Alzheimers Dis* 31(3):475–492
- Kheradmand E, Hajizadeh Moghaddam A, Zare M (2018) Neuroprotective effect of hesperetin and nano-hesperetin on recognition memory impairment and the elevated oxygen stress in rat model of Alzheimer's disease. *Biomed Pharmacother* 97:1096–1101
- Klementiev B, Novikova T, Novitskaya V, Walmod PS, Dmytriyeva O, Pakkenberg B, Berezin V, Bock E (2007) A neural cell adhesion molecule-derived peptide reduces neuropathological signs and cognitive impairment induced by Aβ_{25–35}. *Neuroscience* 145(1):209–224 (**Epub 2007 Jan 16. Erratum in: Neuroscience. 2014 Apr 25;266:136–7**)
- Knezovic A, Osmanovic-Barilar J, Curlin M, Hof PR, Simic G, Riederer P, Salkovic-Petrisic M (2015) Staging of cognitive deficits and neuropathological and ultrastructural changes in streptozotocin-induced rat model of Alzheimer's disease. *J Neural Transm (Vienna)* 122(4):577–592
- Knezovic A, Loncar A, Homolak J, Smailovic U, Osmanovic Barilar J, Ganoci L, Bozina N, Riederer P, Salkovic-Petrisic M (2017) Rat brain glucose transporter-2, insulin receptor and glial expression are acute targets of intracerebroventricular streptozotocin: risk factors for sporadic Alzheimer's disease? *J Neural Transm (Vienna)* 124(6):695–708
- Kraska A, Santin MD, Dorieux O, Joseph-Mathurin N, Bourrin E, Petit F, Jan C, Chaigneau M, Hantraye P, Lestage P, Dhenain M (2012) In vivo cross-sectional characterization of cerebral alterations induced by intracerebroventricular administration of streptozotocin. *PLoS One* 7(9):e46196
- Kreutzberg GW (1996) Microglia: a sensor for pathological events in the CNS. *Trends Neurosci* 19(8):312–318
- Lannert H, Hoyer S (1998) Intracerebroventricular administration of streptozotocin causes long-term diminutions in learning and memory abilities and in cerebral energy metabolism in adult rats. *Behav Neurosci* 112(5):1199–1208
- Llorens-Martín M, Blazquez-Llorca L, Benavides-Piccione R, Rabano A, Hernandez F, Avila J, DeFelipe J (2014) Selective alterations of neurons and circuits related to early memory loss in Alzheimer's disease. *Front Neuroanat* 27:8:38
- Majkutewicz I, Kurowska E, Podlacha M, Myślińska D, Grembecka B, Ruciński J, Plucińska K, Jerzemowska G, Wrona D (2016a) Dimethyl fumarate attenuates intracerebroventricular streptozotocin-induced spatial memory impairment and hippocampal neurodegeneration in rats. *Behav Brain Res* 308. <https://doi.org/10.1016/j.bbr.2016.04.012>
- Majkutewicz I, Kurowska E, Podlacha M, Myślińska D, Grembecka B, Ruciński J, Plucińska K, Jerzemowska G, Wrona D (2016b) Dimethyl fumarate attenuates intracerebroventricular streptozotocin-induced spatial memory impairment and hippocampal neurodegeneration in rats. *Behav Brain Res* 308:24–37
- Mayer G, Nitsch R, Hoyer S (1990) Effects of changes in peripheral and cerebral glucose metabolism on locomotor activity, learning and memory in adult male rats. *Brain Res* 532(1–2):95–100
- McGeer EG, McGeer PL (2003) Inflammatory processes in Alzheimer's disease. *Prog Neuropsychopharmacol Biol Psychiatry* 27(5):741–749
- Mehla J, Pahuja M, Gupta YK (2013) Streptozotocin-induced sporadic Alzheimer's disease: selection of appropriate dose. *J Alzheimers Dis* 33(1):17–21
- Montgomery DL (1994) Astrocytes: form, functions, and roles in disease. *Vet Pathol* 31(2):145–167 (**Review**)
- Morel GR, Andersen T, Pardo J, Zuccolilli GO, Cambiaggi VL, Hereñú CB, Goya RG (2015) Cognitive impairment and morphological changes in the dorsal hippocampus of very old female rats. *Neuroscience* 303:189–199
- Nanfaro F, Cabrera R, Bazzocchini V, Laconi M, Yunes R (2010) Pregnenolone sulfate infused in lateral septum of male rats impairs novel object recognition memory. *Pharmacol Rep* 62(2):265–272
- Nayak D, Roth TL, McGavern DB (2014) Microglia development and function. *Annu Rev Immunol* 32:367–402. <https://doi.org/10.1146/annurev-immunol-032713-120240> (**Epub 2014 Jan 22. Review**)
- Nunomura A, Castellani RJ, Zhu X, Moreira PI, Perry G, Smith MA (2006) Involvement of oxidative stress in Alzheimer disease. *J Neuropathol Exp Neurol* 65(7):631–641 (**Review**)
- Ozkay UD, Can OD, Ozkay Y, Oztürk Y (2012) Effect of benzothiazole/piperazine derivatives on intracerebroventricular streptozotocin-induced cognitive deficits. *Pharmacol Rep* 64(4):834–847
- Padurariu M, Ciobica A, Mavroudis I, Fotiou D, Baloyannis S (2012) Hippocampal neuronal loss in the CA1 and CA3 areas of Alzheimer's disease patients. *Psychiatr Danub* 24(2):152–158
- Pardo J, Abba MC, Lacunza E, Francelle L, Morel GR, Outeiro TF, Goya RG (2017) Identification of a conserved gene signature associated with an exacerbated inflammatory environment in the hippocampus of aging rats. *Hippocampus* 27(4):435–449
- Pathan AR, Viswanad B, Sonkusare SK, Ramarao P (2006) Chronic administration of pioglitazone attenuates intracerebroventricular streptozotocin induced-memory impairment in rats. *Life Sci* 79(23):2209–2216
- Paxinos G, Watson C (1998) The rat brain in stereotaxic coordinates. Academic Press, San Diego
- Perry VH, Nicoll JA, Holmes C (2010 Apr) Microglia in neurodegenerative disease. *Nat Rev Neurol* 6(4):193–201 (**Review**)
- Pompl PN, Mullan MJ, Bjugstad K, Arendash GW (1999) Adaptation of the circular platform spatial memory task for mice: use in detecting cognitive impairment in the APP(SW) transgenic mouse model for Alzheimer's disease. *J Neurosci Methods* 87(1):87–95
- Querfurth HW, LaFerla FM (2010) Alzheimer's disease. *N Engl J Med* 362(4):329–344
- Rajasekar N, Nath C, Hanif K, Shukla R (2017) Intranasal insulin improves cerebral blood flow, Nrf-2 expression and BDNF in STZ (ICV)-induced memory impaired rats. *Life Sci* 173:1–10
- Rodrigues L, Dutra MF, Ilha J, Biasibetti R, Quincozes-Santos A, Leite MG, Marcuzzo S, Achaval M, Gonçalves CA (2010) Treadmill training restores spatial cognitive deficits and neurochemical alterations in the hippocampus of rats submitted to an intracerebroventricular administration of streptozotocin. *J Neural Transm (Vienna)* 117(11):1295–1305
- Rodríguez-Arellano JJ, Parpura V, Zorec R, Verkhratsky A (2016) Astrocytes in physiological aging and Alzheimer's disease. *Neuroscience* 323:170–182
- Rosenfeld CS, Ferguson SA (2014) Barnes maze testing strategies with small and large rodent models. *J Vis Exp* 26(84):e51194
- Rostami F, Javan M, Moghimi A, Haddad-Mashadrizh A, Fereidoni M (2017) Streptozotocin-induced hippocampal astrogliosis and insulin signaling malfunction as experimental scales for subclinical sporadic Alzheimer model. *Life Sci* 188:172–185
- Salkovic-Petrisic M, Hoyer S (2007) Central insulin resistance as a trigger for sporadic Alzheimer-like pathology: an experimental approach. *J Neural Transm Suppl* 72:217–233 (**Review**)
- Salkovic-Petrisic M, Osmanovic J, Grünblatt E, Riederer P, Hoyer S (2009) Modeling sporadic Alzheimer's disease: the insulin resistant brain state generates multiple long-term morphobiological abnormalities including hyperphosphorylated tau protein and amyloid-beta. *J Alzheimers Dis* 18(4):729–750 (**Review**)

- Salkovic-Petrisic M, Osmanovic-Barilar J, Brückner MK, Hoyer S, Arendt T, Riederer P (2011) Cerebral amyloid angiopathy in streptozotocin rat model of sporadic Alzheimer's disease: a long-term follow up study. *J Neural Transm (Vienna)* 118(5):765–772
- Salkovic-Petrisic M, Knezovic A, Hoyer S, Riederer P (2013) What have we learned from the streptozotocin-induced animal model of sporadic Alzheimer's disease, about the therapeutic strategies in Alzheimer's research. *J Neural Transm (Vienna)* 120(1):233–252
- Salkovic-Petrisic M, Knezovic A, Osmanovic-Barilar J, Smailovic U, Trkulja V, Riederer P, Amit T, Mandel S, Youdim MB (2015) Multi-target iron-chelators improve memory loss in a rat model of sporadic Alzheimer's disease. *Life Sci* 136:108–119
- Saxena G, Patro IK, Nath C (2011) ICV STZ induced impairment in memory and neuronal mitochondrial function: a protective role of nicotinic receptor. *Behav Brain Res* 224(1):50–57
- Schubert M, Gautam D, Surjo D, Ueki K, Baudler S, Schubert D, Kondo T, Alber J, Galldiks N, Küstermann E, Arndt S, Jacobs AH, Krone W, Kahn CR, Brüning JC (2004) Role for neuronal insulin resistance in neurodegenerative diseases. *Proc Natl Acad Sci USA* 101(9):3100–3105
- Selkoe DJ (2001) Alzheimer's disease: genes, proteins, and therapy. *Physiol Rev* 81(2):741–766 (**Review**)
- Senitz D, Reichenbach A, Smith TG Jr (1995) Surface complexity of human neocortical astrocytic cells: changes with development, aging, and dementia. *J Hirnforsch* 36:531–537
- Shayan Amiri A, Haj-Mirzaian M, Momeny H, Amini-Khoei M, Rahimi-Balaei S, Poursaman M, Vahid N, Tahmineh M (2017) Streptozotocin induced oxidative stress, innate immune system responses and behavioral abnormalities in male mice. *Neuroscience* 340:373–383
- Shi L, Zhang Z, Li L, Hölscher C (2017) A novel dual GLP-1/GIP receptor agonist alleviates cognitive decline by re-sensitizing insulin signaling in the Alzheimer icv. STZ rat model. *Behav Brain Res* 327:65–74
- Shoham S, Bejar C, Kovalev E, Weinstock M (2003) Intracerebroventricular injection of streptozotocin causes neurotoxicity to myelin that contributes to spatial memory deficits in rats. *Exp Neurol* 184(2):1043–1052
- Shoham S, Bejar C, Kovalev E, Schorer-Apelbaum D, Weinstock M (2007) Ladostigil prevents gliosis, oxidative-nitrate stress and memory deficits induced by intracerebroventricular injection of streptozotocin in rats. *Neuropharmacology* 52(3):836–843
- Sholl DA (1953) Dendritic organization in the neurons of the visual and motor cortices of the cat. *J Anat* 87(4):387–406
- Song J, Hur BE, Bokara KK, Yang W, Cho HJ, Park KA, Lee WT, Lee KM, Lee JE (2014) Agmatine improves cognitive dysfunction and prevents cell death in a streptozotocin-induced Alzheimer rat model. *Yonsei Med J* 55(3):689–699
- Stoub TR, deToledo-Morrell L, Stebbins GT, Leurgans S, Bennett DA, Shah RC (2006) Hippocampal disconnection contributes to memory dysfunction in individuals at risk for Alzheimer's disease. *Proc Natl Acad Sci USA* 103(26):10041–10045
- Streit WJ, Mrak RE, Griffin WS (2004) Microglia and neuroinflammation: a pathological perspective. *J Neuroinflammation* 1(1):14
- Su L, Hayes L, Soteriades S, Williams G, Brain SAE, Firbank MJ, Longoni G, Arnold RJ, Rowe JB (2018) Hippocampal stratum radiatum, lacunosum, and moleculare sparing in mild cognitive impairment. *J Alzheimers Dis* 61(1):415–424
- Uriarte M, Ogundele OM, Pardo J (2017) Long-lasting training in the Barnes maze prompts hippocampal spinogenesis and habituation in rats. *Neuroreport* 28(6):307–312
- Vijayan VK, Geddes JW, Anderson KJ, Chang-Chui H, Ellis WG, Cotman CW (1991) Astrocyte hypertrophy in the Alzheimer's disease hippocampal formation. *Exp Neurol* 112(1):72–78
- West MJ. West MJ (1993) New stereological methods for counting neurons. *Neurobiol Aging* 14(4):275–285 (**Review**)
- West MJ, Coleman PD, Flood DG, Troncoso JC (1994) Differences in the pattern of hippocampal neuronal loss in normal ageing and Alzheimer's disease. *Lancet* 17(8925):769–772
- Wirhns O, Bayer TA (2010) Neuron Loss in Transgenic Mouse Models of Alzheimer's Disease. *Int J Alzheimer's Dis* 723782